

## Renormalization of the effective mass deduced from the period of microwave-induced resistance oscillations in GaAs/AlGaAs heterostructures

A. V. Shchepetilnikov,<sup>1</sup> D. D. Frolov,<sup>1</sup> Yu. A. Nefyodov,<sup>1</sup> I. V. Kukushkin,<sup>1</sup> and S. Schmult<sup>2</sup>

<sup>1</sup>*Institute of Solid State Physics RAS, 142432 Chernogolovka, Moscow district, Russia*

<sup>2</sup>*Max-Planck-Institut für Festkörperforschung, Heisenbergstraße 1, 70569 Stuttgart, Germany*

(Received 3 February 2017; published 17 April 2017)

The microwave-induced resistance oscillations were studied in a number of GaAs/AlGaAs quantum wells and heterojunctions of various electron sheet densities  $n$ . The effective mass  $m^*$  extracted from the oscillations period demonstrated strong nonmonotonic dependence on  $n$ . At low densities  $m^*$  was greatly enhanced (heavier than the cyclotron mass) and abruptly decreased with increasing  $n$ . Such behavior exhibited by the effective mass at low  $n$  is clearly of many-particle origin. The minimal values of  $m^*$  were observed at moderate densities and were lower than the cyclotron mass in full consistency with earlier publications by other groups. The increase of the effective mass observed at high densities can be ascribed to the nonparabolicity of the conduction band.

DOI: [10.1103/PhysRevB.95.161305](https://doi.org/10.1103/PhysRevB.95.161305)

At low temperatures longitudinal magnetoresistance of a high-quality two-dimensional electron system (2DES) irradiated by microwave radiation exhibits well-developed oscillations [1–3] periodic in the reciprocal magnetic field. In contrast to the well-known Shubnikov–de Haas oscillations their period is governed by the commensurability of the cyclotron energy and microwave frequency. This phenomenon, traditionally referred to as microwave-induced resistance oscillations (MIRO), was first observed almost 20 years ago in charged GaAs/AlGaAs quantum wells and its discovery was followed by extensive experimental and theoretical efforts reviewed, e.g., in Ref. [4].

Although a number of well-elaborated theories [5–14] were presented to account for MIRO, there are still several crucial aspects of the phenomenon they fail to explain. The complete immunity of MIRO to the helicity of the incident microwave radiation should be mentioned as one of the brightest examples [15,16]. Another important issue is the reduction of the effective mass deduced from the MIRO period (traditionally referred to as MIRO mass) if compared to the cyclotron mass [17]. Note that the observed discrepancy exceeds by far the experimental accuracy of the mass determination both from MIRO and cyclotron resonance. The present Rapid Communication aims to address this issue experimentally. The effective MIRO mass  $m^*$  is shown to undergo pronounced renormalization due to the strong electron-electron interaction, as  $m^*$  turned out to increase abruptly with decreasing electron sheet densities  $n$  at low  $n$ —the dependence clearly reminiscent of the Fermi-liquid quasiparticle mass behavior.

MIRO were observed in different geometries of the contacts including conventional Hall bar [1,3], Corbino ring [18,19], and Van der Pauw geometry [20,21], even with the aid of contactless techniques [22,23] and in different material systems including electrons on a liquid-helium surface [24,25],  $p$ -type Ge/SiGe quantum well [26], and MgZnO/ZnO heterojunctions [27]. Similar oscillations have been observed recently in the magnetocapacitance of a 2DES [28]. The microwave-induced contribution  $\delta\rho$  to the longitudinal magnetoresistance of a 2DES channel at low magnetic fields is conveniently expressed as [4]

$$\delta\rho \sim -A \exp(-\alpha\epsilon) \sin(2\pi\epsilon + \delta), \quad (1)$$

where  $\epsilon$  is a ratio of the microwave frequency  $f$  to the value  $f_c^* = eB/m^*$  ( $e$  stands for the electron charge and  $B$  for the magnetic field). It is tempting to refer to  $f_c^*$  as a cyclotron frequency, yet the effective mass  $m^*$  calculated from the MIRO period is considerably lower than the mass extracted from the cyclotron resonance magnetic field dispersion. The phase of the oscillations is typically zero and thus the magnetic field positions of the MIRO minima and maxima are governed by a simple rule traditionally referred to as “1/4 cycle shift”:  $\epsilon = i \mp 1/4$ , where  $i \in \mathbb{N}$  [29–31]. Nonzero phase was observed for low-order oscillation numbers  $i$  in ultraclean samples [30]. The exponential factor in Eq. (1) represents the damping of MIRO oscillations with the dampening factor  $\alpha$  being proportional to the quantum scattering rate  $1/\tau_q$  [32]. The amplitude  $A$  of the oscillations grows with the microwave power  $P$ : linearly at low  $P$  and  $\propto P^{1/2}$  at higher power [33]. Provided the power of the incident on 2DES microwave radiation is high enough and the temperature is low, the minima of several low-order oscillations tend to transform into states with zero diagonal resistance [3,20]; this process is accompanied by a formation of current domains [34–36].

Our experiments were performed on a number of GaAs/AlGaAs quantum wells and heterojunctions with electron sheet densities varying from  $0.6$  to  $6.2 \times 10^{11} \text{ cm}^{-2}$  characterized by similar electron mobilities in the range of  $1\text{--}2 \times 10^6 \text{ cm}^2/\text{Vs}$  at  $T = 1.5 \text{ K}$ . Standard Hall bars with source, drain, and several sense contacts were lithographically formed on the samples.

The microwave-induced part of the 2DES longitudinal magnetoresistance was precisely measured with the aid of a conventional double lock-in technique. An ac probe current of an amplitude  $\sim 1 \mu\text{A}$  at a frequency  $f_{ac} \sim 1 \text{ kHz}$  was applied from source to drain. The first lock-in amplifier monitored the channel resistance  $R_{xx}$  through two sense contacts along the channel. The sample was irradiated by microwaves 100% amplitude modulated at a frequency  $f_{mod} \sim 30 \text{ Hz}$  and guided to the sample via a rectangular oversized waveguide. A microwave generator with frequency multipliers coupled to it was used as the radiation source, providing the experimentally available frequency range up to 140 GHz. The second lock-in amplifier, synchronized at  $f_{mod}$ , was connected to the output of the first one and, thus, measured the variation  $\delta R_{xx}$  in the

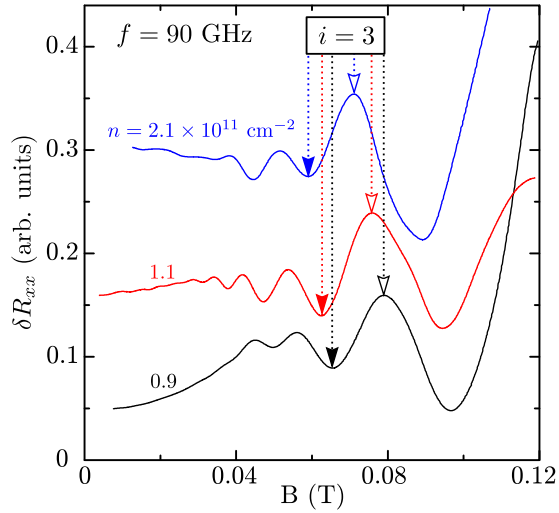


FIG. 1. The microwave-induced part of the 2DES longitudinal magnetoresistance measured in three samples with different sheet densities  $n = 0.9$  (black line),  $1.1$  (red line), and  $2.1 \times 10^{11} \text{ cm}^{-2}$  (blue line). Arrows indicate the positions of MIRO minimum and maximum corresponding to  $i = 3$ . The data is shifted along vertical axis for clarity. The microwave frequency equaled 90 GHz for all of the three samples.

magnetoresistance, caused by the microwave irradiation. The samples were placed inside of the 1.5-K pot of the  $^4\text{He}$  cryostat and the experiments were carried out under liquid-helium pumping.

Typical dependences of the microwave-induced part of the 2DES longitudinal resistance on the magnetic field  $B$  measured in three samples with different sheet densities  $n = 0.9$ ,  $1.1$ , and  $2.1 \times 10^{11} \text{ cm}^{-2}$  are presented in Fig. 1. Microwave frequency was equal to 90 GHz. The shift of the MIRO extrema position toward lower magnetic fields with the increase of the electron density can be clearly seen. According to Eq. (1) this experimental observation suggests that the effective MIRO mass decreases with the increase of  $n$ .

Since the exact magnetic field position of the MIRO extrema is influenced by the phase  $\delta$ , the value of  $\delta$  has to be checked carefully. The conventional value of the phase  $\delta = 0$  was adopted first; as a result, according to Eq. (1) the magnetic field positions of the MIRO extrema should occur at  $\epsilon = i \mp 1/4$ . Then the reciprocal magnetic fields of the MIRO maxima and minima against  $i \mp 1/4$ , respectively, were plotted for a given frequency  $f = 90 \text{ GHz}$  of the microwave radiation. The described procedure is illustrated in Fig. 2 for two samples with densities  $n = 0.9$  and  $2.1 \times 10^{11} \text{ cm}^{-2}$ . All the experimental data points turned out to be well fitted with straight lines described by a simple equation  $i \mp 1/4 = 2\pi f m^* / eB$ . The effective MIRO masses extracted from the slopes of the lines in Fig. 2 were equal to  $m^* = 0.067m_0$  and  $m^* = 0.060m_0$  for  $n = 0.9$  and  $2.1 \times 10^{11} \text{ cm}^{-2}$ . As all the lines started from the point of origin for each of the samples studied, the previously made assumption of zero phase was correct within the experimental accuracy. The slopes of the lines were dependent on the electron sheet density highlighting the dependence of the effective MIRO mass on  $n$ .

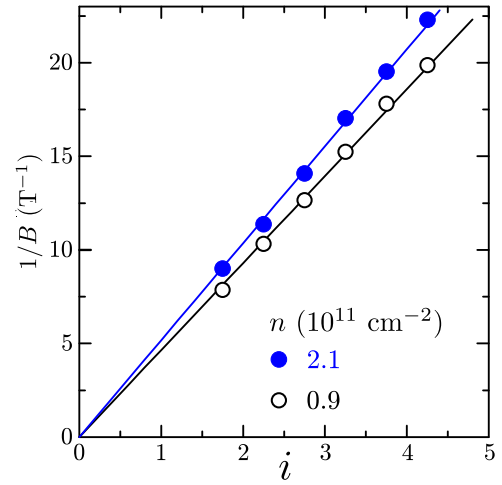


FIG. 2. The dependence of the reciprocal magnetic fields correspondent to the MIRO extrema on  $i \mp 1/4$  for two samples with  $n = 0.9$  (open circles) and  $2.1 \times 10^{11} \text{ cm}^{-2}$  (solid circles). The experimental data is fitted perfectly with the straight lines  $i \mp 1/4 = 2\pi f m^* / eB$  through the point of origin. The microwave frequency equaled 90 GHz for both samples.

It is now established that the effective MIRO mass does depend on the electron sheet density with the exact dependence having been acquired as follows. For each sample the microwave-induced part of the magnetoresistance was measured in the whole experimentally available frequency range. The exact magnetic field positions of MIRO maxima and minima for a given  $i$  were plotted as microwave frequency dispersions  $f(B)$ . The first low-order extrema, typically 1 and 2, were overlapped by Shubnikov–de Haas oscillations and were not taken into account when the MIRO effective mass was extracted. For each sample the experimental dispersions of the  $i$ th MIRO extrema were fitted by straight lines according to the formula  $f = (i - 1/4)eB/2\pi m^*$  for maxima and  $f = (i + 1/4)eB/2\pi m^*$  for minima. Note that for each sample the parameter  $m^*$ , extracted from the slopes of these lines, was the same for all the oscillation numbers used for fitting and, thus, do represent the effective MIRO mass.

Figure 3 demonstrates example dispersions  $f(B)$  of the MIRO minima corresponding to oscillation numbers  $i = 3, 4$  for three samples with the electron sheet density  $n = 0.9$ ,  $1.1$ , and  $2.1 \times 10^{11} \text{ cm}^{-2}$ . For a given oscillation number  $i$  the experimental dispersions are well fitted with straight lines. The lines do not coincide for all three samples, as their slopes are clearly dependent on the sample electron density. Moreover, the slopes tend to increase with growing  $n$  clearly indicating that MIRO effective mass  $m^*$  does rise with the decrease of  $n$ . The exact values of  $m^*$  measured for these samples are presented in Fig. 3.

The resulting effective MIRO mass dependence on the electron density is presented in Fig. 4 (blue solid circles). The value of  $m^* = 0.0587m_0$  measured in the sample with the density  $n = 2.7 \times 10^{11} \text{ cm}^{-2}$  in Ref. [17] denoted in the figure (red open circle) is consistent with our results. The observed dependence is not monotonic: with the increase of  $n$  the value of  $m^*$  decreases quickly at low densities, whereas it rises slowly at higher  $n$ . To understand such

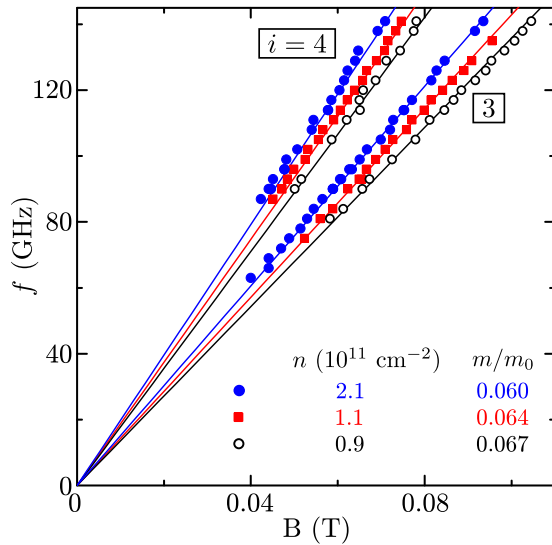


FIG. 3. Dispersions  $f(B)$  of the several selected MIRO minima  $i = 3, 4$  for three samples with the electron sheet density  $n = 0.9, 1.1,$  and  $2.1 \times 10^{11} \text{ cm}^{-2}$ . Straight lines represent fits according to the formula  $f = (i + 1/4)eB/2\pi m^*$  with  $i = 3, 4$ . Corresponding effective masses  $m^*$  are denoted in the figure for each of the samples.

peculiar behavior we compare the effective MIRO mass  $m^*$  with two other types of masses: mass determined from the electron cyclotron resonance dispersion (black open triangles) and the Fermi-liquid quasiparticle mass (black open squares), namely, quasiparticle density of states effective mass, measured simultaneously in Ref. [37] with high accuracy for various electron densities of the 2DES. At low densities the behavior exhibited by MIRO mass and mass of Fermi-liquid quasiparticle is essentially the same: they both rise abruptly with the  $n$  decrease. Such similarity suggests the observed enhancement of MIRO mass at low  $n$  to be the result of the mass renormalization due to the strong electron-electron interaction. Note that the density-dependent electron mass determined from detailed low-temperature Shubnikov-de Haas measurements in GaAs/AlGaAs heterostructures exhibits analogous rising behavior at low  $n$  [38]. The slow rise of  $m^*$  at large densities is identical to the rise exhibited by the cyclotron resonance effective mass and, thus, can be attributed to the nonparabolicity of the GaAs electron spectrum [37,39]. At moderate densities MIRO mass is still considerably reduced compared to the cyclotron mass; such reduction was previously ascribed to the effects of electron-electron interaction [17] as well.

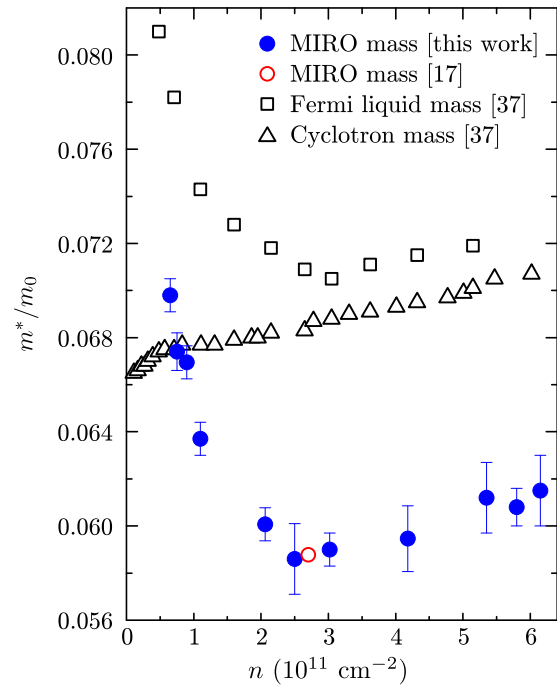


FIG. 4. The experimental dependence of the effective MIRO mass on the electron sheet density (blue closed circles). The value of  $m^* = 0.0587m_0$  measured in the sample with the density  $n = 2.7 \times 10^{11} \text{ cm}^{-2}$  in Ref. [17] is denoted by the red open circle. Open triangles and squares represent the electron density dependences of the mass determined from cyclotron resonance dispersion and quasiparticle Fermi-liquid mass adopted from Ref. [37].

In conclusion, the microwave photoresistance was studied in a series of GaAs/AlGaAs quantum wells and heterojunctions with different densities  $n$  of 2DES. The effective mass  $m^*$  deduced from the MIRO period was lighter than the cyclotron mass at moderate densities in full consistency with earlier publications by other groups. In contrast, the value of  $m^*$  turned out to be enhanced at low densities. The observed enhancement of MIRO mass is clearly the result of the mass renormalization due to the strong electron-electron interactions. This experimental finding points out the need for further theoretical efforts, as it cannot be accounted for by any existing single-particle theoretical approaches. The increase of the effective mass exhibited at high densities can originate from the conduction-band nonparabolicity.

We gratefully acknowledge the financial support from the Russian Science Foundation (Grant No. 14-12-00599).

- [1] M. A. Zudov, R. R. Du, J. A. Simmons, and J. L. Reno, *Phys. Rev. B* **64**, 201311 (2001).
- [2] P. D. Ye, L. W. Engel, D. C. Tsui, J. A. Simmons, J. R. Wendt, G. A. Vawter, and J. L. Reno, *Appl. Phys. Lett.* **79**, 2193 (2001).
- [3] R. G. Mani, J. H. Smet, K. von Klitzing, V. Narayana-murti, W. B. Johnson, and V. Umansky, *Nature (London)* **420**, 646 (2002).

- [4] I. A. Dmitriev, A. D. Mirlin, D. G. Polyakov, and M. A. Zudov, *Rev. Mod. Phys.* **84**, 1709 (2012).
- [5] Adam C. Durst, Subir Sachdev, N. Read, and S. M. Girvin, *Phys. Rev. Lett.* **91**, 086803 (2003).
- [6] X. L. Lei and S. Y. Liu, *Phys. Rev. Lett.* **91**, 226805 (2003).
- [7] M. G. Vavilov and I. L. Aleiner, *Phys. Rev. B* **69**, 035303 (2004).
- [8] S. I. Dorozhkin, *JETP Lett.* **77**, 577 (2003).

- [9] I. A. Dmitriev, A. D. Mirlin, and D. G. Polyakov, *Phys. Rev. Lett.* **91**, 226802 (2003).
- [10] I. A. Dmitriev, M. G. Vavilov, I. L. Aleiner, A. D. Mirlin, and D. G. Polyakov, *Phys. Rev. B* **71**, 115316 (2005).
- [11] A. D. Chepelianskii and D. L. Shepelyansky, *Phys. Rev. B* **80**, 241308(R) (2009).
- [12] O. V. Zhironov, A. D. Chepelianskii, and D. L. Shepelyansky, *Phys. Rev. B* **88**, 035410 (2013).
- [13] S. A. Mikhailov, *Phys. Rev. B* **83**, 155303 (2011).
- [14] Y. M. Beltukov and M. I. Dyakonov, *Phys. Rev. Lett.* **116**, 176801 (2016).
- [15] J. H. Smet, B. Gorshunov, C. Jiang, L. Pfeiffer, K. West, V. Umansky, M. Dressel, R. Meisels, F. Kuchar, and K. von Klitzing, *Phys. Rev. Lett.* **95**, 116804 (2005).
- [16] T. Herrmann, I. A. Dmitriev, D. A. Kozlov, M. Schneider, B. Jentsch, Z. D. Kvon, P. Olbrich, V. V. Bel'kov, A. Bayer, D. Schuh, D. Bougeard, T. Kuczuk, M. Oltcher, D. Weiss, and S. D. Ganichev, *Phys. Rev. B* **94**, 081301(R) (2016).
- [17] A. T. Hatke, M. A. Zudov, J. D. Watson, M. J. Manfra, L. N. Pfeiffer, and K. W. West, *Phys. Rev. B* **87**, 161307(R) (2013).
- [18] C. L. Yang, M. A. Zudov, T. A. Knuttila, R. R. Du, L. N. Pfeiffer, and K. W. West, *Phys. Rev. Lett.* **91**, 096803 (2003).
- [19] A. A. Bykov, *JETP Lett.* **87**, 233 (2008).
- [20] M. A. Zudov, R. R. Du, L. N. Pfeiffer, and K. W. West, *Phys. Rev. Lett.* **90**, 046807 (2003).
- [21] A. A. Bykov, D. R. Islamov, A. V. Goran, and A. K. Bakarov, *JETP Lett.* **86**, 779 (2007).
- [22] A. A. Bykov, I. V. Marchishin, A. V. Goran, and D. V. Dmitriev, *Appl. Phys. Lett.* **97**, 082107 (2010).
- [23] I. V. Andreev, V. M. Muravev, I. V. Kukushkin, S. Schmult, and W. Dietsche, *Phys. Rev. B* **83**, 121308(R) (2011).
- [24] D. Konstantinov and K. Kono, *Phys. Rev. Lett.* **103**, 266808 (2009).
- [25] R. Yamashiro, L. V. Abdurakhimov, A. O. Badrutdinov, Yu. P. Monarkha, and D. Konstantinov, *Phys. Rev. Lett.* **115**, 256802 (2015).
- [26] M. A. Zudov, O. A. Mironov, Q. A. Ebner, P. D. Martin, Q. Shi, and D. R. Leadley, *Phys. Rev. B* **89**, 125401 (2014).
- [27] D. F. Karcher, A. V. Shchepetilnikov, Yu. A. Nefyodov, J. Falson, I. A. Dmitriev, Y. Kozuka, D. Maryenko, A. Tsukazaki, S. I. Dorozhkin, I. V. Kukushkin, M. Kawasaki, and J. H. Smet, *Phys. Rev. B* **93**, 041410(R) (2016).
- [28] S. I. Dorozhkin, A. A. Kapustin, V. Umansky, K. von Klitzing, and J. H. Smet, *Phys. Rev. Lett.* **117**, 176801 (2016).
- [29] R. G. Mani, J. H. Smet, K. von Klitzing, V. Narayanamurti, W. B. Johnson, and V. Umansky, *Phys. Rev. Lett.* **92**, 146801 (2004).
- [30] M. A. Zudov, *Phys. Rev. B* **69**, 041304(R) (2004).
- [31] A. T. Hatke, M. A. Zudov, L. N. Pfeiffer, and K. W. West, *Phys. Rev. B* **84**, 241304(R) (2011).
- [32] I. A. Dmitriev, M. Khodas, A. D. Mirlin, D. G. Polyakov, and M. G. Vavilov, *Phys. Rev. B* **80**, 165327 (2009).
- [33] A. T. Hatke, M. Khodas, M. A. Zudov, L. N. Pfeiffer, and K. W. West, *Phys. Rev. B* **84**, 241302(R) (2011).
- [34] A. A. Bykov, *JETP Lett.* **91**, 361 (2010).
- [35] S. I. Dorozhkin, L. Pfeiffer, K. West, K. von Klitzing, and J. H. Smet, *Nat. Phys.* **7**, 336 (2011).
- [36] I. A. Dmitriev, M. Khodas, A. D. Mirlin, and D. G. Polyakov, *Phys. Rev. Lett.* **111**, 206801 (2013).
- [37] I. V. Kukushkin and S. Schmult, *JETP Lett.* **101**, 693 (2015).
- [38] Y.-W. Tan, J. Zhu, H. L. Stormer, L. N. Pfeiffer, K. W. Baldwin, and K. W. West, *Phys. Rev. Lett.* **94**, 016405 (2005).
- [39] M. A. Hopkins, R. J. Nicholas, M. A. Brummell, J. J. Harris, and C. T. Foxon, *Phys. Rev. B* **36**, 4789 (1987).